Ali, Utku Emre; Yang, He; Khayrudinov, Vladislav; Modi, Gaurav; Cheng, Zengguang; Agarwal, Ritesh; Lipsanen, Harri; Bhaskaran, Harish

A Universal Pick-and-Place Assembly for Nanowires

Published in:
Small

DOI:
10.1002/smll.202201968

Published: 22/09/2022

Document Version
Publisher's PDF, also known as Version of record

NANO · MICRO small
www.small-journal.com

A Universal Pick-and-Place Assembly for Nanowires

*Utku Emre Ali, He Yang, Vladislav Khayrudinov, Gaurav Modi, Zengguang Cheng, Ritesh Agarwal, Harri Lipsanen, and Harish Bhaskaran**

With the introduction of techniques to grow highly functional nanowires of exotic materials and demonstrations of their potential in new applications, techniques for depositing nanowires on functional platforms have been an area of active interest. However, difficulties in handling individual nanowires with high accuracy and reliability have so far been a limiting factor in large-scale integration of high-quality nanowires. Here, a technique is demonstrated to transfer single nanowires reliably on virtually any platform, under ambient conditions. Functional nanowires of InP, AlGaAs, and GeTe on various patterned structures such as electrodes, nanophotonic devices, and even ultrathin transmission electron microscopy (TEM) membranes are transferred. It is shown that the versatility of this technique further enables to perform on-chip nano-optomechanical measurements of an InP nanowire for the first time via evanescent field coupling. Thus, this technique facilitates effortless integration of single nanowires into applications that were previously seen as cumbersome or even impractical, spanning a wide range from TEM studies to in situ electrical, optical, and mechanical characterization.

1. Introduction

For almost two decades, nanowires have been employed as functional devices in nanoelectronics and nanophotonics due to their fascinating electrical[1] and optical[2] properties, yet their integration at the physical device level remains elusive. Reliable integration becomes even more challenging when it comes to creating unique devices of single nanowires such as low-noise photodetectors,[3] ultra-low-power memory elements,[4] and nonvolatile frequency tuners.[5] Some approaches for the assembly of 1D nanostructures include stamping methods,[6–8] atomic force microscopy based manipulation,[9,10] solution drop-dry technique,[11] lithographic alignment,[12] the Langmuir-Blodgett process,[13,14] and localized growth of nanowires at predetermined nucleation points.[15] Among all these methods, only the stamp-transfer technique, if improved, has the potential to be a universal tool for nanowire deposition[1] owing to its material-independent methodology as well as the controllability of density and orientation.[7] Crucially, this technique allows ex-post-facto placement of functional nanowires, which would enable their integration into mass-produced components that may otherwise be sensitive to solvents or nanowire growth processes.

In the stamping technique, nanowires are transferred from a growth substrate to an intermediate transparent and elastic medium, termed stamp, which is then contact-printed on the device substrate under a light microscope. One major drawback of this method is the absence of a nanoscale tool that can pick up desired nanowires from the growth substrate. Generally, the stamp is pressed onto the growth substrate, which results in collecting a "forest" of nanowires in a random fashion.[6,8] This greatly increases fabrication complexity (e.g., additional lithography steps) and reduces reproducibility especially for applications that require a single nanowire placement with high precision. In addition, the design of the stamp needs revisiting since conventional flat stamps[6] have to be perfectly parallel to the device substrate without leaving a headroom for misalignment (tilt). Even when complete tilt correction is performed, there is still uncertainty about which part of the relatively large stamp is imprinted on the microscale device, inevitably lengthening the fabrication process. Here, we describe and demonstrate a process that allows the stamping technique to reach its full potential by significantly increasing single nanowire placement precision and enhancing reproducibility.

U. E. Ali, Z. Cheng,[+] H. Bhaskaran
Department of Materials
University of Oxford
Oxford OX1 3PH, UK
E-mail: harish.bhaskaran@materials.ox.ac.uk
H. Yang
School of Instrumentation and Optoelectronic Engineering
Beihang University
Beijing 100191, China
V. Khayrudinov, H. Lipsanen
Department of Electronics and Nanoengineering
Aalto University
Espoo FI-00076, Finland
G. Modi, R. Agarwal
Department of Materials Science and Engineering
University of Pennsylvania
Philadelphia, PA 19104, USA
The ORCID identification number(s) for the author(s) of this article can be found under https://doi.org/10.1002/smll.202201968.

[+]Present address: State Key Laboratory of ASIC and System, School of Microelectronics, Fudan University, Shanghai 200433, China

DOI: 10.1002/smll.202201968

2. Results and Discussion

The design of nanoscale tools for picking up individual nanowires is not dissimilar to cranes used in forestry to move logs. However, the physics acting at the nanoscale is different. With scaling, surface interactions such as adhesive forces (i.e., van der Waals interactions) dominate the force fields.[16] Therefore, performing the picking-up step requires a comprehensive understanding of adhesion. It is well-known that soft materials are less abrasive and adhere better to rigid bodies due to their viscoelasticity allowing them to spread around surfaces.[16,17] Hence, instead of using inorganic materials such as tungsten tips,[18] we choose polyethylene terephthalate (PET) monofilaments in our process.

To match the monofilament dimensions with nanowires, we taper the filament reducing its thickness from 200 µm to sub-micron levels by using a purpose-built heat-and-pull setup (**Figure 1**a). In order to control pulling parameters, i.e., pull length and velocity, the monofilament is fixed on a 1D motorized stage. The temperature of the hot surface is set to 240 °C. By bringing the polymer into close contact with the hot surface, the monofilament is melted. Subsequent pulling of the filament away from the hot surface leads to the cooling of the liquid polymer while forming a taper (Video S1, Supporting Information). The thickness of the taper depends mainly on the pulling parameters. Experimental data in Figure 1b shows a clear trend that the diameter of the tapered tip can be decreased down to 0.38 µm by increasing pull length and velocity to 12 mm and 7 mm s^{-1}, respectively. This is the first example of a polymer tip with sub-micron diameter,[19] and its micromachining does not involve lithography steps unlike nanoscale tips of inorganic materials.[9,18,20]

Figure 2a depicts the single-nanowire picking-up process using the sub-micron tip mounted on a 5-axis micromanipulator. When the separation between the tip and the nanowire is below ≈10 nm, they jump into contact due to van der Waals attractions.[16] Employing such surface interactions further makes the picking-up step material-independent. We have also observed that as long as the tip diameter is below ≈2 µm, the resulting ad hoc tool can reproducibly pick up single nanowires with diameters of 120–400 nm (Figure S1, Supporting Information) with a significant yield of ≈80%, substantially relaxing the parameters for the heat-and-pull process. We should also mention that the lower limit for the nanowire diameter in our case is restricted by the resolution of optical microscopy. For photonics applications, this limit needs to be pushed below 100 nm,[21] and we believe that this can be achieved in future by using novel metalens structures with ultrahigh numerical aperture.[22]

Following the picking-up step, the nanowire is transferred onto the center of a transparent polydimethylsiloxane (PDMS) stamp (Figure 2b). PDMS has served as a universal material in stamping technology mainly due to its elasticity and transparency as well as facile preparation. Here, we have further engineered the stamp design to ensure greater reliability and accuracy. PDMS droplets are cured upside-down on a glass slide in order to form a dome-shaped stamp with a diameter of ≈2 mm (Experimental Section), without necessitating complicated processes such as micro-stamping[23] or vacuum curing.[24] As will be seen, the dome shape allows the nanowire to be placed faster with high precision.[24]

Then, the glass slide is fixed on a 3-axis micromanipulator with the nanowire facing downwards while the device substrate sits on top of the microscope stage (Figure 2c). Following the alignment of the nanowire with the device, the PDMS stamp is contact-printed on the device substrate. The device is then separated from the stamp by lowering the microscope stage, with a slight movement in the direction along the nanowire's growth axis (see Figure S2, Supporting Information). To ensure a successful contact-printing step, one needs to follow this dragging movement. This further eliminates the need for heating the device substrate formerly required to overcome the strong mechanical interlocking between the nanowire and the elastic stamp.[6] Thus, the nanowire transfer is completed in less than 3 min (Figure 2d). The whole process is further demonstrated in Video S2 (Supporting Information). Given that all existing nanowire stamping techniques require additional lithography steps, such a short duration in our method is unequivocally superior.

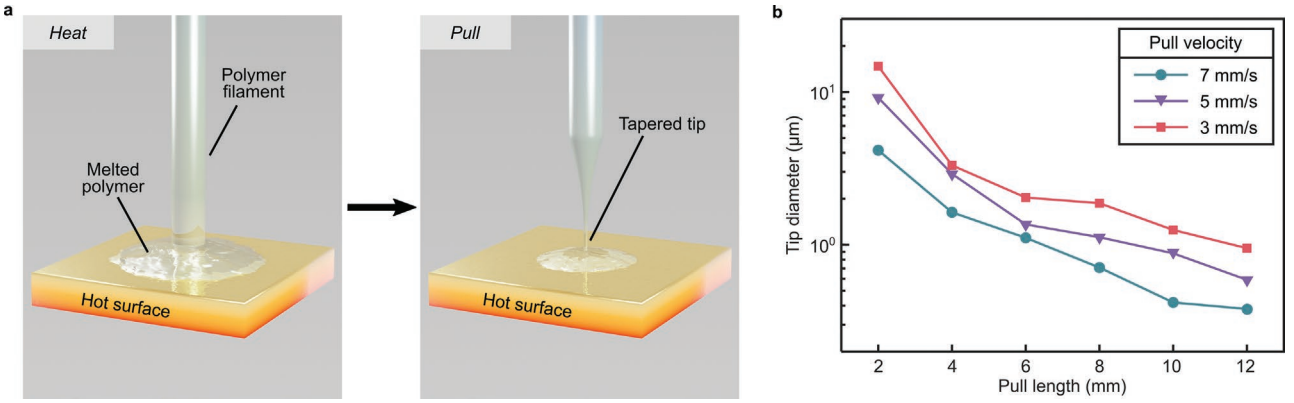

Figure 1. Tapering of a polymer monofilament. a) Schematic of the heat-and-pull setup designed for fabricating the nano-crane. A polymer filament (PET, a diameter of 200 µm) is attached on an automated micromanipulator and melted on a clean and polished hot surface at 240 °C. By pulling operation, the melted polymer on the surface instantly cools down and forms a taper. b) Graph showing the characterization of the heat-and-pull setup for various pull lengths and velocities. Increasing pull length and velocity decreases the tip diameter down to sub-micron levels (≈0.4 µm). Video S1 (Supporting Information) shows the formation of the taper.

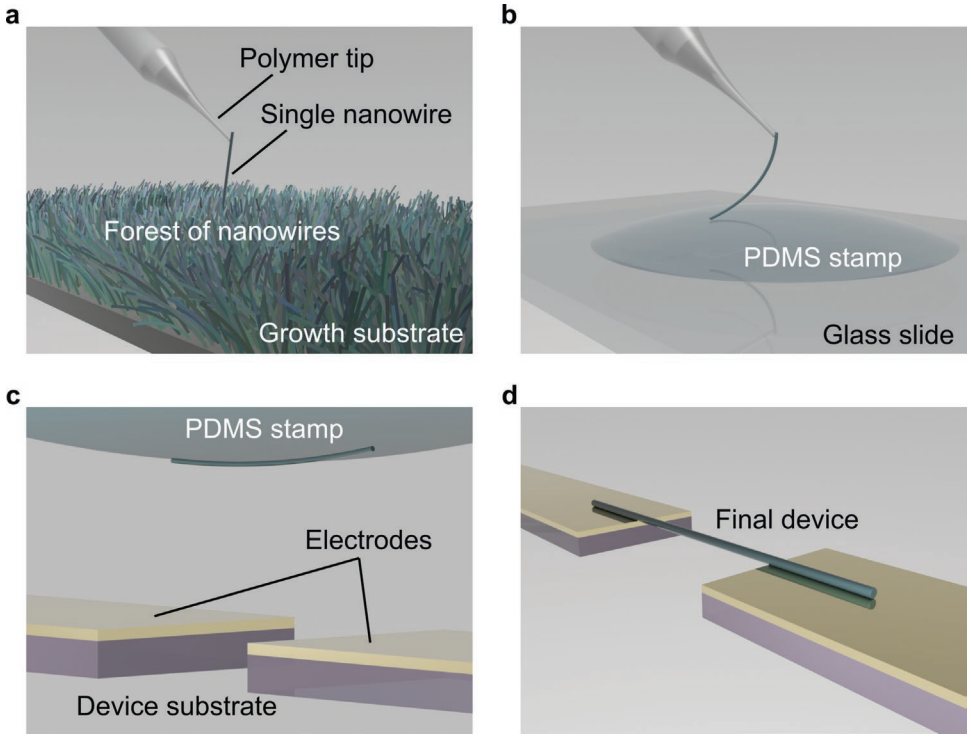

Figure 2. Nanowire transfer process. a) A single nanowire is picked up by the tapered polymer tip from a forest of nanowires on the growth substrate. The nanowire adheres to the tip due to the enhanced van der Waals forces overcoming the weaker interactions between smooth, crystalline nanowire surfaces. b) The nanowire on the tip is placed onto a dome-shaped PDMS stamp cured over a glass slide. Note that the adhesion of the PDMS stamp to the nanowire is greater than that of the tip. c) The stamp with the nanowire is turned upside down and its alignment with the device chip is done under a light microscope. Following alignment, the stamp is imprinted over electrodes on the device substrate. d) Nanowire deposition is completed with the removal of the stamp.

Placement precision of the method has also been characterized. To this end, we have deposited 25 nanowires on Au electrodes. The target position and orientation have been compared to those of the obtained devices (Figure S3, Supporting Information). Analysis results suggest a discrepancy of 0.6 µm in position and 1.2° in orientation, both of which are even suitable for applications in nanophotonics.[2] It should also be noted that in this work, we have only used manual nanopositioners without a rotation stage. We believe using motorized stages with rotation capability in the *xy*-plane will improve the placement precision even further. Besides, based on our experience, the effect of ambient temperature and atmospheric conditions on the placement process is negligible.

At this point, it is crucial to investigate if the technique poses a limitation in terms of nanowire length. On flat substrates, we have not observed a minimum length requirement. However, for most applications, nanowires need to be deposited over patterned substrates with physical gaps, e.g., between two electrodes. In that case, the nanowire needs to be satisfyingly longer than the gap. In practice, we suggest as a rule of thumb that the nanowire length should be at least twice the gap size. As for an upper limit, we have noted that the transferred nanowire starts to have a deformed shape when the length-to-diameter ratio of the nanowire becomes larger than ≈600. While we do not exclude the possibility of extending our method to even longer nanowires,[25] we should mention that maintaining a straight shape would be challenging.

In the case of an electronic device, the chip can be subsequently annealed at 150 °C for 10 min to improve the electrical contact to the nanowire. As such, we prepared electronic devices by depositing individual nanowires of InP, AlGaAs, and GeTe over Au electrodes. Optical micrographs of the relevant devices and their corresponding IV curves are given in **Figure 3**a–c. As can be seen from the data, Au forms Schottky barriers with the extrinsic semiconductor nanowires of InP (unintentional n-type doping)[3,26] and AlGaAs (lightly p-type doped by Zn)[26] while resulting in ohmic contacts with the metallic GeTe nanowire.[27]

We further note that, after annealing, adhesion between the electrodes and the nanowire is remarkably enhanced, i.e., the nanowire remains on the electrodes even in liquid media unless a solution-based sonication is performed. Thus, the nanowires can be functionalized by additional wet chemistry even after the deposition is completed. As an example, we have demonstrated the feasibility of a further lithography step in Figure S3 (Supporting Information), showing the high mechanical stability offered by this technique and enabling the use of exotic nanowires in potential biosensing schemes.[28]

We have also managed to deposit nanowires on fragile substrates such as ultra-thin membranes. In Figure 3d, a GeTe nanowire deposited on a TEM grid made of a 50 nm thick Si_3N_4 membrane can be seen together with the corresponding diffraction pattern of its rhombohedral lattice. This demonstration not only shows the applicability of our method for TEM studies

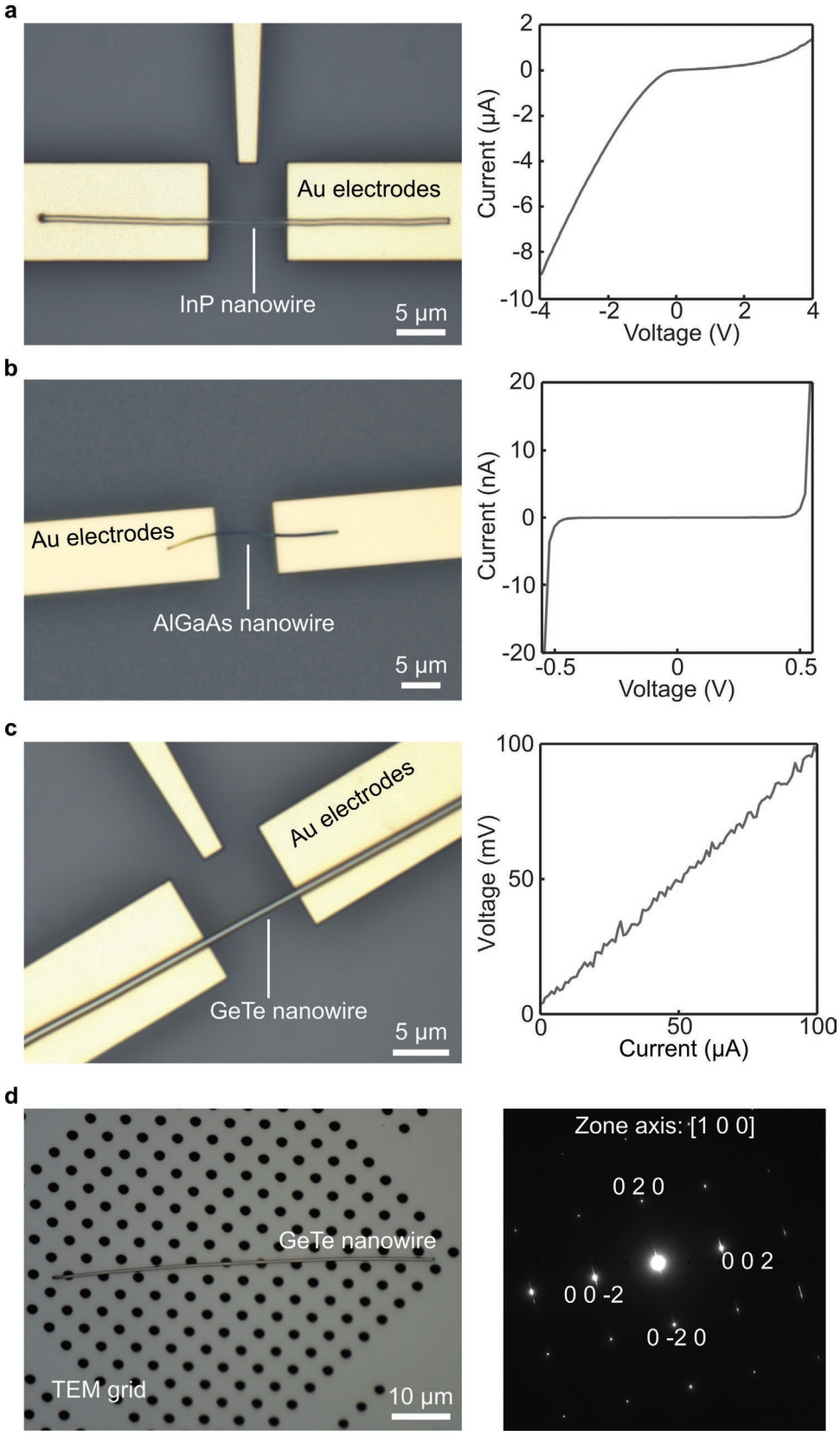

Figure 3. Nanowires deposited on various functional platforms. Freestanding nanowires of a) InP, b) AlGaAs, and c) GeTe on Au electrodes and the corresponding IV curves. d) A GeTe nanowire transferred on a 50 nm thick Si_3N_4 TEM membrane with 2 μm pores, together with the relevant diffraction pattern in TEM.

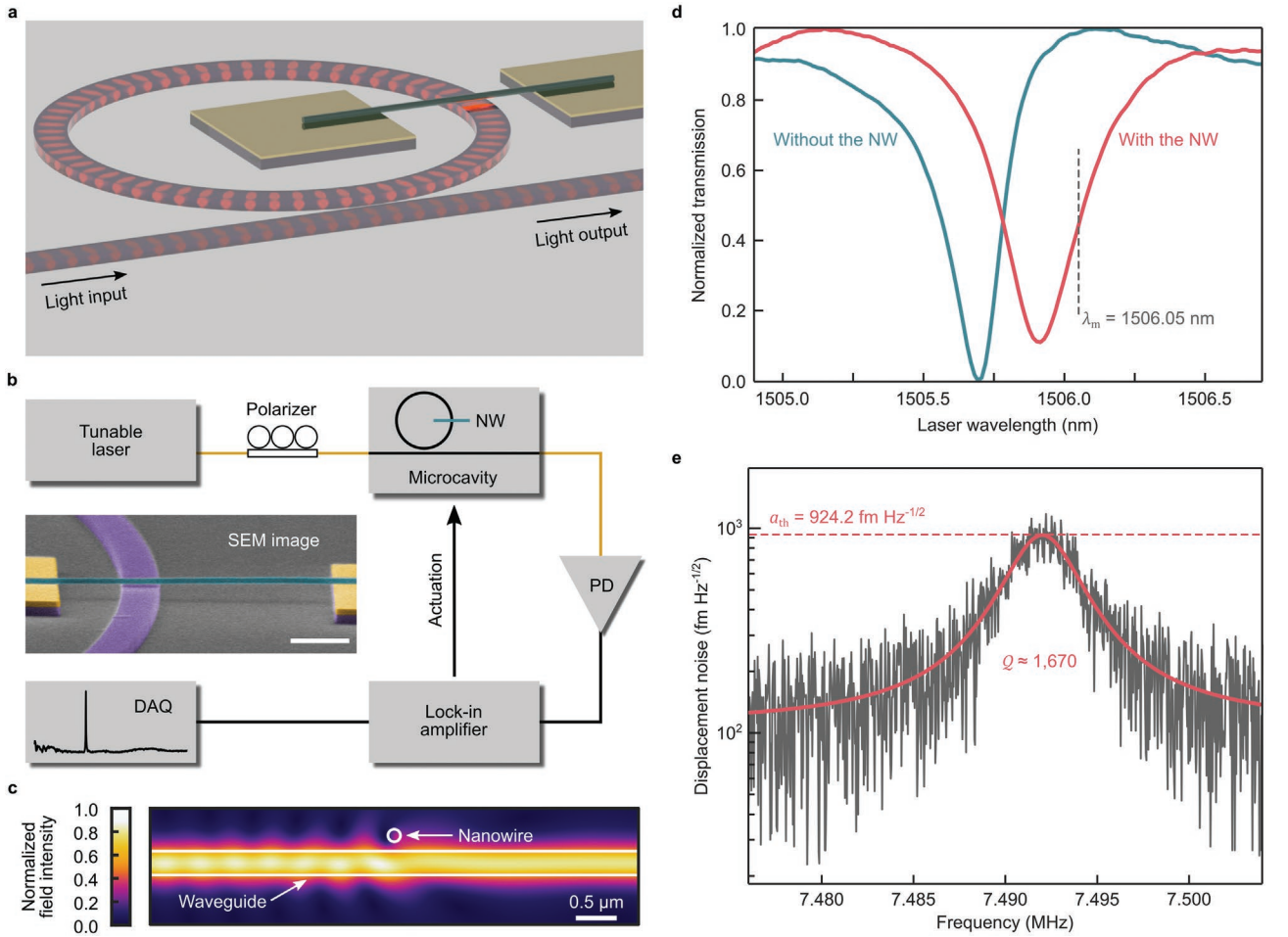

Figure 4. On-chip optomechanical transduction of a doubly-clamped, free-standing InP nanowire (NW). a) Schematic showing the nanowire suspended over an optical microcavity. Light is coupled into the cavity through a photonic waveguide. b) Experiment setup for detecting the nanomechanical resonance. Polarized light excites the cavity mode and the vibrations from the nanowire evanescently induce a change in the optical field. Read-out is performed by a lock-in amplifier that both detects the optical transmission change via a photodiode (PD) and mechanically actuates the resonator. Inset, an angled-view false-color SEM image of the device. Scale bar, 2 μm. c) Optical simulations showing the interaction between the nanowire (InP) and the photonic waveguide (Si_3N_4). The lossy nanowire acts as a scatterer and absorber near the dielectric waveguide. d) Normalized optical cavity transmission before (green, critical coupling) and after (pink) the nanowire deposition. The nanowire introduces additional optical loss to the microcavity, resulting in linewidth broadening. Optomechanical measurements are performed at a wavelength of λ_m. e) Raw experimental data showing the nondriven response (no actuation) of the nanowire for a probe power of 21 μW. The Lorentzian fit (solid pink line) to the thermomechanical noise (1 Hz bandwidth) yields a mechanical quality factor of 1670 with a_{th} its peak value, suggesting a displacement sensitivity of 110.29 fm Hz$^{-1/2}$.

but also reveals the delicacy and versatility of the stamping technique.

Significantly, our method paves the way for first-of-its-kind devices in the nanowire realm. One such application is illustrated in **Figure 4**a, where a doubly clamped InP nanowire is suspended between Au electrodes, 150 nm away from a photonic microcavity of Si_3N_4 (see Experimental Section for fabrication details). As estimated from the scanning electron microscope (SEM) image in the inset of Figure 4b, the nanowire has a length of L = 9.2 μm and a diameter of D = 150 nm. By combining this platform with the experiment setup given in Figure 4b, nanomechanical vibrations of the nanowire can be probed via evanescent field coupling[20] with excellent sensitivity.

We start with exciting the optical cavity mode using polarized light from a tunable laser source. As indicated by the optical field profile in Figure 4c, the nanowire acts as a lossy scatterer over the waveguide.[29] The experimental data in Figure 4d further confirms that the nanowire perturbs the optical mode of the microcavity by altering the critical-coupling condition and broadening the linewidth. In order to obtain the displacement spectrum of the InP nanowire, we set the laser wavelength at the positive-slope side of the optical cavity mode (λ_m = 1506.05 nm).

Non-driven, thermomechanical response of the resonator (Figure 4e, spectral density, 1 Hz bandwidth) is obtained with a probe power of 21 μW (see Figure S5, Supporting Information for the driven responses). The Lorentzian fit to the thermomechanical noise data yields a quality factor Q = 1670 and a resonance frequency f_0 = 7.492 MHz. The measured Young's modulus of the InP nanowire (E = 122 GPa) is in good agreement with previously reported values.[30] We further calibrate

the displacement sensitivity[31] of the measurement using the thermomechanical peak value (a_{th}) of the resonator[32] :

$$a_{th} \approx \sqrt{\frac{4k_B TQ}{m_{eff}(2\pi f_0)^3}} \quad (1)$$

Here, m_{eff} is the effective mass of the resonator, k_B is the Boltzmann constant, and T is ambient temperature. From here, the displacement sensitivity for a probe power of 21 µW is calculated as 110.29 fm $Hz^{-1/2}$ (see Experimental Section for how this is estimated).

As this is the first cavity optomechanics study of a single-crystal nanowire, it is also important to provide a theoretical relation between optomechanical coupling and the design parameters. Optomechanical coupling rate (g_{om}) is defined as the microcavity resonance shift per unit motion of the nanomechanical resonator, i.e., $g_{om} = \partial\omega_c/\partial z_0$, where ω_c is the microcavity resonance and z_0 is the vertical distance between the nanowire and the microcavity. Using cavity perturbation theory,[33] one can reach the following relation in the case of out-of-plane vibrations of a nanowire resonator:

$$g_{om} = \omega_c(n_{nano}^2 - 1)\xi^2 e^{-2\alpha z_0} e^{-\alpha D} \frac{w}{V_{cav}} \int_{-D/2}^{D/2} \sinh(2\alpha\sqrt{D^2/4 - x^2})\mathrm{d}x \quad (2)$$

Here, n_{nano} is the refractive index of the nanowire (assuming a lossless dielectric), ξ is the normalized field amplitude at the vacuum/cavity intersection, α is the evanescent decay rate, D is the nanowire diameter, V_{cav} is the effective mode volume of the cavity, and ω is the width of the cavity waveguide. Our experiments suggest a g_{om} of 75 MHz nm^{-1}, which is in a good agreement of 7% with the theoretical value. Equation (2) further suggests that g_{om} can be improved by using a nanowire with higher refractive index or a larger diameter, a shorter nanowire/cavity distance, a smaller cavity volume, and a higher optical (cavity) resonance frequency.

In fact, the readout amplitude is not only determined by g_{om} but also affected by other parameters such as the quality factor of the cavity and the optical probe power.[20,32,33] For example, for the same amount of optical resonance shift ($\partial\omega_c$), i.e., constant g_{om}, a cavity with a higher quality factor (narrower linewidth) will result in a greater optical intensity variation. Similarly, when the field strength in the cavity becomes larger for a higher probe power, and a larger change will be observed at the output. For the latter case, we have provided further experimental data in Figure S6 (Supporting Information), which shows the thermomechanical noise for various probe powers together with the corresponding displacement sensitivity. Remarkably, the displacement sensitivity gets as good as 34.44 fm $Hz^{-1/2}$ for a probe power of 75 µW.

Previous work by Barnard et al.[20] demonstrated nanomechanical vibrations of a carbon nanotube, which was evanescently coupled to a discrete photonic cavity element using microtweezers. The transduction method described in our work offers up to 20× improvement in terms of displacement sensitivity. We mainly attribute this to the better noise performance of our fully integrated transduction approach, which would otherwise be impractical without this pick-and-place technique. Note that, in practice, the transduction efficiency can be further enhanced by using higher probe powers, reducing z_0, improving the fiber-to-chip coupling efficiency (Experimental Section) and/or the quality factor of the microcavity.

3. Conclusion

In conclusion, we present a complete pick-and-place assembly that can handle individual nanowires with high precision and reproducibility. Using this basic approach, we create disparate devices that can readily be employed in electrical, optical, mechanical, and even crystallographic characterization of exotic nanowires. We further describe a powerful methodology, for the first time, for fully-integrated photonic transduction of mechanical resonators of single, pristine nanowires. As such, we envisage that the novel nanomanufacturing tools described here will speed up the advances in nanowire research inexpensively by allowing users to incorporate nanowires with existing on-chip platforms, be it electronic or photonic, elucidating device physics to an extent that has not been attainable so far. Complete automation of this assembly is possible, and so is the ability to do so on a wafer-scale with multiple stamps and global alignment markers, making full-scale fabrication of high quality, CVD-grown, nanowire-integrated chips a real possibility.

4. Experimental Section

Heat-and-Pull Setup: The polymer monofilament (Goodfellow Polyethylene Terephthalate Monofilament) was manipulated by a 1D motorized stage (PI L-511 High-Precision Linear Stage), and the pulling parameters were controlled by the device software. The hot surface was formed using a temperature-controlled soldering iron tip.

Preparation of PDMS Stamps: The two-part liquid kit (SYLGRAD 184) was used for preparing the stamps. The mix ratio was selected as 10:1 as suggested by the manufacturer, without performing de-airing. Glass slides were cleaned with ethanol and the elastomer mixture was carefully transferred onto the glass slide surface forming circular droplets with diameters of 2–3 mm. The glass slides were kept upside-down throughout the process, preventing the liquid mixture from spreading out. Then, they were placed on a hot plate (90 °C) facing down and cured for an hour. When not used, the stamps can be stored at room temperature for at least 4 months, without losing their ability as a transfer medium.

Nanowire Synthesis: InP and AlGaAs nanowires were grown on Si (111) substrates using a horizontal flow atmospheric pressure metalorganic vapor phase epitaxy (MOVPE) system.[26] Trimethylindium (TMIn), tertiarybutylphosphine (TBP), trimethylaluminum (TMAl), trimethylgallium (TMGa), and tertiarybutylarsine (TBAs) were used as precursors. Au nanoparticles (NPs) with diameters of 60 nm and 40 nm (BBI International, UK) were used as catalysts for the vapor-liquid-solid (VLS) growth. Poly-L-Lysine (PLL) solution was applied to the substrate for better NP adhesion followed by the deposition of Au NPs. The substrates were annealed in situ at 650 °C for 10 min under hydrogen flow to desorb surface contaminants before the growth. The growth temperature of InP NWs was 430 °C for 300 s and the nominal V/III ratio was ≈200. The growth temperature of AlGaAs NWs was 450 °C for 300 s and the nominal V/III ratio was ≈8. Hydrogen was used as a carrier gas, and the total reactor gas flow rate was ≈5 L min^{-1} (slm). GeTe nanowires were synthesized by a catalyst-assisted VLS growth mechanism.[27] A few milligrams of GeTe powder (Alfa Aesar, 99.999% purity) were placed at the center of a tube furnace (Lindberg/Blue M). A Si substrate sputtered with a thin film of Au–Pd (≈5 nm) was placed at ≈5 in. upstream from the center. Ar gas was purged into the chamber to remove any residual

oxygen until reaching a pressure of 30 mTorr. The base pressure in the furnace was then stabilized at 100 Torr while maintaining the Ar flow rate at 100 sccm. Subsequently, the temperature of the furnace was ramped up to 650 °C and the nanowire synthesis was carried out for an hour before the furnace was gradually cooled down to room temperature.

Nanofabrication of the Photonic Chip: The photonic platform (inset of Figure 4b) within two electron-beam lithography (EBL, JEOL 5500FS) steps was manufactured. A 10×10 mm^2 piece diced from a Si wafer with a thin layer of Si_3N_4 (0.33 µm) on top of a 3 µm thick oxide layer. The first EBL step was used to deposit Cr/Au electrodes (150 nm in total) by thermal evaporation. In the second step, waveguides were patterned (1.3 µm wide) using MaN-2403 negative resist. The patterns were then transferred on the Si_3N_4 thin film by reactive ion etching (RIE, Oxford 80 Plasmalab) in CHF_3/O_2/Ar mixture, with the electrodes acting as a hard mask. Thus, the height difference between the waveguide and the anchoring points of the nanowire was defined as 150 nm.

Fiber-to-Chip Coupling: The tunable probe laser (Santec TSL-550) was polarized (Thorlabs FPC032) and coupled into the on-chip microcavity via grating couplers. The gratings were designed to selectively couple the TE mode of the waveguide. The fiberoptic array (from SQS Vlaknova optika a.s.) was aligned with the grating couplers for maximum efficiency (≈10% per coupler). Following the alignment, the fiber array was mechanically fixed on the chip-carrying platform using epoxy (Araldite Rapid Drying Epoxy Resin) and cured overnight. Then, the resulting portable platform was placed in a vacuum chamber.

Nano-Optomechanical System Characterization: Frequency response of the InP nanowire resonator was acquired using a lock-in amplifier (Zurich Instruments HF2LI). Vibrational (out-of-plane) mode of the resonator was actuated through direct mechanical coupling using a piezoceramic shaker (Thorlabs PA4FEW). The actuator was driven by the lock-in system through a power amplifier (Mini Circuits LZY-22+). Read-out signal was obtained and amplified via a battery-powered, ultralow noise fiberoptic receiver (Newport 1811-FC). All measurements were performed at room temperature and in vacuum environment (≈10^{-6} mbar).

Estimation of Displacement Sensitivity: For a probe power of 21 µW, the Lorentzian fit yields a peak voltage noise of 210.352 nV Hz$^{-1/2}$ and a voltage noise floor of 24.926 nV Hz$^{-1/2}$ (see Figure S6 in the Supporting Information). Here, the peak height (208.87 nV Hz$^{-1/2}$) is a result of the thermomechanical vibrations of the nanowire at resonance, which can be theoretically calculated from Equation (1) as 924.228 fm Hz$^{-1/2}$. Thus, the transduction gain is computed as 208.87 nV Hz$^{-1/2}$/924.228 fm Hz$^{-1/2}$ ≈ 0.226 nV fm^{-1}. Using this gain value, one can estimate the minimum resolvable displacement value by converting the off-resonance voltage noise floor to the displacement domain: 24.926 nV Hz$^{-1/2}$/0.226 nV fm^{-1} ≈ 110.29 fm Hz$^{-1/2}$, which simply yields the displacement sensitivity.

Supporting Information

Supporting Information is available from the Wiley Online Library or from the author.

Acknowledgements

The authors thank Nathan Youngblood, Benjamin F. Porter, Jia Hao Eugene Soh, and A.Ne for their valuable inputs during discussions. V.K. acknowledges the support of Aalto University Doctoral School, Walter Ahlström Foundation, Elektroniikkainsinöörien Säätiö, Sähköinsinööriliiton Säätiö, Nokia Foundation, Finnish Foundation for Technology Promotion (Tekniikan Edistämissäätiö), Waldemar von Frenckell's foundation and Kansallis-Osake-Pankki fund, and the EU H2020-MSCA-RISE-872049 (IPN-Bio). V.K. and H.L. acknowledge financial support from Academy of Finland Flagship Programme (320167, PREIN) and the technical support by Aalto University at Micronova Nanofabrication Centre. R.A. and G.M. were supported by the ONR-MURI, grant #N00014-17-1-2661. UEA was supported by The Scientific and Technological Research Council of Turkey (TÜBİTAK) and the Department of Materials, University of Oxford. H.B. acknowledges long-term support from EPSRC (grants EP/J00541X/2, EP/M015173/1, EP/T023899/1, EP/J018694/1, and EP/R001677/1).

Conflict of Interest

The authors declare no conflict of interest.

Data Availability Statement

The data that support the findings of this study are available in the supplementary material of this article.

Keywords

cavity optomechanics, nanostructures, nanowires, pick-and-place

Received: March 29, 2022
Revised: June 6, 2022
Published online: August 8, 2022

[1] W. Lu, C. M. Lieber, *Nat. Mater.* **2007**, *6*, 841.
[2] R. Yan, D. Gargas, P. Yang, *Nat. Photonics* **2009**, *3*, 569.
[3] X. Yan, B. Li, Y. Wu, X. Zhang, X. Ren, *Appl. Phys. Lett.* **2016**, *109*, 053109.
[4] S.-H. Lee, Y. Jung, R. Agarwal, *Nat. Nanotechnol.* **2007**, *2*, 626.
[5] U. E. Ali, G. Modi, R. Agarwal, H. Bhaskaran, *Nat. Commun.* **2022**, *13*, 1464.
[6] Y. Lu, M. Stegmaier, P. Nukala, M. A. Giambra, S. Ferrari, A. Busacca, W. H. P. Pernice, R. Agarwal, *Nano Lett.* **2017**, *17*, 150.
[7] A. Javey, Nam, R. S. Friedman, H. Yan, C. M. Lieber, *Nano Lett.* **2007**, *7*, 773.
[8] Z. Fan, J. C. Ho, Z. A. Jacobson, R. Yerushalmi, R. L. Alley, H. Razavi, A. Javey, *Nano Lett.* **2008**, *8*, 20.
[9] H. Xie, D. S. Haliyo, S. Régnier, *Nanotechnology* **2009**, *20*, 215301.
[10] M. Moreno-Moreno, P. Ares, C. Moreno, F. Zamora, C. Gómez-Navarro, J. Gómez-Herrero, *Nano Lett.* **2019**, *19*, 5459.
[11] D. Li, Y. Wu, R. Fan, P. Yang, A. Majumdar, *Appl. Phys. Lett.* **2003**, *83*, 3186.
[12] M. Bockrath, *Science* **1997**, *275*, 1922.
[13] P. Yang, *Nature* **2003**, *425*, 243.
[14] D. Whang, S. Jin, Y. Wu, C. M. Lieber, *Nano Lett.* **2003**, *3*, 1255.
[15] R. He, D. Gao, R. Fan, A. I. Hochbaum, C. Carraro, R. Maboudian, P. Yang, *Adv. Mater.* **2005**, *17*, 2098.
[16] K. Kendall, *Science* **1994**, *263*, 1720.
[17] B. A. Latella, B. K. Gan, C. J. Barbé, D. J. Cassidy, *J. Mater. Res.* **2008**, *23*, 2357.
[18] I. E. Zadeh, A. W. Elshaari, K. D. Jöns, A. Fognini, D. Dalacu, P. J. Poole, M. E. Reimer, V. Zwiller, *Nano Lett.* **2016**, *16*, 2289.
[19] D. F. Merchant, P. J. Scully, N. F. Schmitt, *Sens. Actuators, A* **1999**, *76*, 365.
[20] A. W. Barnard, M. Zhang, G. S. Wiederhecker, M. Lipson, P. L. McEuen, *Nature* **2019**, *566*, 89.
[21] Y. Sun, X. Xie, Y. Chen, B. Sun, C. Wang, *ACS Nano* **2019**, *13*, 772.
[22] H. Liang, Q. Lin, X. Xie, Q. Sun, Y. Wang, L. Zhou, L. Liu, X. Yu, J. Zhou, T. F. Krauss, J. Li, *Nano Lett.* **2018**, *18*, 4460.

[23] R. A. Hemnani, J. P. Tischler, C. Carfano, R. Maiti, M. H. Tahersima, L. Bartels, R. Agarwal, V. J. Sorger, *2D Mater.* **2018**, *6*, 015006.
[24] D. Rosser, T. Fryett, A. Saxena, A. Ryou, A. Majumdar, A. Majumdar, *Opt. Mater. Express* **2020**, *10*, 645.
[25] Y. Sun, B. Sun, J. He, G. Yang, C. Wang, *Nat. Commun.* **2020**, *11*, 647.
[26] H. Yang, V. Khayrudinov, V. Dhaka, H. Jiang, A. Autere, H. Lipsanen, Z. Sun, H. Jussila, *Sci. Adv.* **2018**, *4*, eaar7954.
[27] P. Nukala, C.-C. Lin, R. Composto, R. Agarwal, *Nat. Commun.* **2016**, *7*, 10482.
[28] Y. Lu, M. Yang, F. Qu, G. Shen, R. Yu, *Bioelectrochemistry* **2007**, *71*, 211.
[29] C. F. Bohren, D. R. Huffman, *Absorption and Scattering of Light by Small Particles*, John Wiley & Sons, New York **2008**.
[30] M. Dunaevskiy, P. Geydt, E. Lähderanta, P. Alekseev, T. Haggrén, J.-P. Kakko, H. Jiang, H. Lipsanen, *Nano Lett.* **2017**, *17*, 3441.
[31] M. Li, H. X. Tang, M. L. Roukes, *Nat. Nanotechnol.* **2007**, *2*, 114.
[32] S. K. Roy, V. T. K. Sauer, J. N. Westwood-Bachman, A. Venkatasubramanian, W. K. Hiebert, *Science* **2018**, *360*, 1.
[33] G. Anetsberger, O. Arcizet, Q. P. Unterreithmeier, R. Rivière, A. Schliesser, E. M. Weig, J. P. Kotthaus, T. J. Kippenberg, *Nat. Phys.* **2009**, *5*, 909.